A Canonical Response of Precipitation Characteristics to Global Warming from CMIP5 Models

William K.-M. Lau *

Laboratory for Atmospheres, NASA, Goddard Space Flight Center, Greenbelt, MD.

H.-T. Wu

Science Systems and Applications, Inc., Lanham, MD.

K.-M. Kim

Morgan State University, Baltimore, MD.

* Correspondence to: Dr. William K.-M. Lau, Earth Science Division, Atmospheres, Code 613, Building 33, Rm C121, NASA Goddard Space Flight Center, Greenbelt, MD 20771, USA; email: William.K.Lau@nasa.gov

Key Points :

1. A canonical global rainfall response to global warming is found in CMIP5 models
2. Increased heavy rain events and droughts are connected globally under global warming
3. Global warming induced changes in rainfall types are more detectable than in total rainfall

Abstract

In this study, we find from analyses of projections of 14 CMIP5 models a robust, canonical global response in rainfall characteristics to a warming climate. Under a scenario of 1% increase per year of CO_2 emission, the model ensemble projects globally more heavy precipitation ($+7\pm2.4\%K^{-1}$), less moderate precipitation ($-2.5\pm0.6\%K^{-1}$), more light precipitation ($+1.8\pm1.3\%K^{-1}$), and increased length of dry (no-rain) periods ($+4.7\pm2.1\%K^{-1}$). Regionally, a majority of the models project a consistent response with more heavy precipitation over climatologically wet regions of the deep tropics especially the equatorial Pacific Ocean and the Asian monsoon regions, and more dry periods over the land areas of the subtropics and the tropical marginal convective zones. Our results suggest that increased CO_2 emissions induce a global adjustment in circulation and moisture availability manifested in basic changes in global precipitation characteristics, including increasing risks of severe floods and droughts in preferred geographic locations worldwide.

Index terms: Precipitation (1854), Global Climate Models (1626), Water Cycle (1655)

1. Introduction

One of the key findings of the Fourth Assessment Report (AR4) of the Intergovernmental Panel on Climate Change (IPCC) is that "*anthropogenic influences have contributed to intensification of extreme precipitation at the global scale*" [*IPCC*, 2007]. The AR4 also noted that while climate models generally project a global increase in rainfall, the projected rate of change and regional signals are highly uncertain, due to coarse model resolution and inadequate model physics. In recent years, many record breaking heavy rain, and prolonged heat waves and droughts events have been reported worldwide [*Field et al.*, 2012]. This is consistent with a growing body of contemporaneous studies suggesting that there is an increased risk of extreme rain events in a warmer climate [*Allan et al.*, 2010; *Groisman et al*., 2005; *Lau and Wu*, 2007, 2011; *Liu et al*., 2012; *Min et al*., 2011; *O'Gorman and Schneider*, 2009; *Trenberth et al*., 2003; *Trenberth* 2011]. However the regional distribution of the increased extreme rain and attribution of precipitation variability to specific climate forcing are still uncertain, and increasing the confidence of future projection of rainfall pattern remains a challenge [*Kharin et al.*, 2007; *Sun et al.*, 2012]. In preparation for the Fifth Assessment Report (AR5), IPCC has organized the Coupled Model Intercomparison Project Phase 5 (CMIP5), coordinating major international research institutions and groups to conduct climate projection experiments using state-of-the-art models with higher resolution and more realistic physics. The results presented in this paper are based on climate projection experiments from 14 CMIP5 models available at the time of this study. While the 14 models have diverse resolutions (Table S1 in the auxiliary material) and representations of physical, chemical, hydrological and oceanic processes, they are subject to the same set of prescribed GHG emission scenarios [*Taylor*, 2012]. Here, we assess CMIP5 model projections of global and regional rainfall response to greenhouse gases (GHG) warming, specifically to increased CO2 emissions. This study differs from previous global warming rainfall studies in that they were mostly focused on extreme rain, or on severe drought separately based on total rain, while we emphasize the changes in rainfall characteristics (types, intensity and duration), and connections between extreme rain and drought events. We will examine rainfall changes not only in total rain, but also changes in the entire rainfall probability distribution function (PDF), including heavy, moderate, light, and no-rain events.

We analyze the outputs of 14 CMIP5 models based on a 140-year experiment with a prescribed 1% per year increase in CO_2 emission. This rate of CO_2 increase is comparable to that prescribed for the RCP8.5, a relatively conservative business-as-usual scenario [*Riahi et al.*, 2011], except the latter includes also changes in other GHG and aerosols, besides CO_2. A 27-year period at the beginning of the integration is used as the control to compute rainfall and temperature statistics, and to compare with climatology (1979–2005) of rainfall data from the Global Precipitation Climatology Project (GPCP). Two similar 27-year periods in the experiment that correspond approximately to a doubling of CO_2 emissions (DCO2) and a tripling of CO_2 emissions (TCO2) compared to the control are chosen respectively to compute the same statistics (for details, see Section S1 in the auxiliary material). The rainfall response to global warming is defined as the difference in the statistics between the control and DCO2, and TCO2 respectively. Since the responses based on DCO2 and TCO2 are similar except with stronger and more robust signal in the latter, unless otherwise stated, results presented are for TCO2.

2. Model rainfall climatology

The rainfall PDFs and cumulative PDFs (CPDFs) for rainfall occurrences and amount, as well as climatological global, and zonal mean rainfall distributions for the model ensemble mean have been computed and found to be in reasonable agreement with GPCP and Tropical Rainfall

Measuring Mission (TRMM) observations (see Section S2 and Fig. S1 in the auxiliary material).

To facilitate discussion regarding rainfall characteristics in this work, we define, based on the ensemble model PDF, three major rain types: light rain (LR), moderate rain (MR), and heavy rain (HR) respectively as those with monthly mean rain rate below the 20th percentile (<0.3 mm/day), between the 40–70th percentile (0.9–2.4 mm/day), and above the 98.5% percentile (> 9 mm/day). An extremely heavy rain (EHR) type defined at the 99.9th percentile (> 24 mm day^{-1}) will also be referred to, as appropriate. The geographic distributions of the three rain types agree quite well between the model ensemble mean and GPCP (Fig. S2 and Section S2 in the auxiliary material), with HR most dominant over the deep convection zone of the tropics, and monsoon regions, MR over midlatitude storm tracks over the continents and the Southern Oceans, and LR over the desert and semi-arid zones, and the subtropical stratocumulus region off the west coast of the Americas and South Africa. Previous studies [*Lau and Wu* 2007; 2011] have found that based on a similar classification, LR, MR and HR can be identified with rainfall subsystems dominated by warm-rain/low clouds, mixed-phase/congestus, and ice-phase rain/deep convection respectively in the tropics. Hence, to a first order approximation, the aforementioned rain types provide a natural separation of rainfall subsystems associated with major climatic regimes. It should also be pointed out that the rain type definition used here is based on global scaling with monthly mean data to facilitate a global narrative. Obviously, this definition has limitations and cannot be used for detailed regional or singular extreme event applications, for which a local relative scaling, with daily or hourly rainfall should be used.

3. Response in total rainfall

All models show a clear increase in global (60°S–60°N) mean temperature due to increased CO_2 emissions, with a rate of 0.2–0.36 K decade^{-1} among models, and an ensemble mean of 0.26 K decade^{-1} (Fig. 1a). Similarly, all models exhibit a clear upward trend in the annual global mean precipitation, with an ensemble mean rate of 0.012 mm $\text{day}^{-1}\text{decade}^{-1}$ or 0.38% decade^{-1} (Fig. 1b). In the zonal mean, most models show increased rainfall in the deep tropics (10°S–10°N) and mid-to-high latitudes (Fig. 1c). Reduced rainfall is found in the subtropics, more pronounced in the Southern Hemisphere (SH) than the Northern Hemisphere (NH), with large variability among models. The model ensemble response (Fig. 1d) shows three distinct zones of rainfall increase: 10°S–10°N, south of 45°S, and north of 40°N; a wide rainfall-reduction zone near 10°S–40°S, and a rainfall-neutral zone near 20°N–40°N. These signals are highly significant (>95–99% c.l.) based on a Student-t test, in the deep tropics and high ($>45^{o}$) latitudes, but less so in the subtropics. Additional analyses of zonal mean profiles over selected longitudinal sectors (Section S3 and Fig. S3 in the auxiliary material) show rainfall reduction in the NH subtropics over North America, and the Europe-Africa sectors, but enhancement over the subtropical central Pacific and Asian monsoon sectors. These regional rainfall anomalies compensate to produce in the zonal mean a near neutral zone over the NH subtropics (Fig. 1d). The rainfall anomalies are consistent with observations of a narrowing of the deep convection zone in the tropics, and a widening of the subtropical belt in recent decades [*Seidel et al.,* 2008; *Hu and Fu*, 2007; *Zhou et al.*, 2011].

Globally, rainfall increases by 4.5%, with a sensitivity (dP/P/dT) of 1.4 % K^{-1} (Table S2 in the auxiliary material), substantially lower than the 7% K^{-1} increase in saturated water vapor governed by the Clausius-Clapeyron relation, consistent with previous findings [*Held and Soden*, 2006; *Andrews et al.*, 2010; *Frieler et al.*, 2011; *Vecchi et al.*, 2006; Giorgi et al., 2011]. The highest sensitivity +6.3% K^{-1} is found over southern mid-to-high-latitudes (50–80°S). The northern mid-to-high-latitudes (50–80°N) and the equatorial region (10°S–10°N) also show high (+3% K^{-1}) sensitivity. Negative sensitivity is found over the NH subtropics, SH subtropics and mid-latitudes, suggesting the importance of large-scale circulation forcing and dynamical feedback [*Lau and Wu*, 2011; *Chou et al.*, 2012].

4. Changes in rainfall characteristics

The changes in rainfall characteristics are analyzed based on the monthly PDFs of rainfall frequency of occurrences (FOC) (Fig. 2a) and amount (Fig. 2b). The ensemble-mean FOC (Fig. 2a, line graphs in logarithmic scale) clearly show that there is a tendency for increase in HR events globally due to CO_2 warming. However, the logarithmic scale in the mean FOC plot masks changes in lower rain rates. For a different perspective, the FOC difference plot (Fig. 2a, bar chart) displays a consistent and robust model response *i.e.*, more HR, less MR and more LR. When the rainfall sensitivity is plotted as a function of rain types, a systematic, canonical pattern in response to CO_2 warming is evident, *i.e., higher positive sensitivity for increasingly heavy rain, negative sensitivity for moderate rain, and positive sensitivity for light rain* (Fig. 2b). The sensitivity is quite high (4–10% K^{-1}) for HR bins (9–15 mm day^{-1}), and increases dramatically (30–100% K^{-1}) for EHR bins (> 24 mm day^{-1}). For MR and LR bins, the sensitivity is negative 2–4% and positive 1–4% K^{-1}, respectively. Analyses of changes of rainfall PDFs over land, ocean separately, and for different latitudinal zones (Section S4 and Fig. S4 in the auxiliary material) show that the same canonical rainfall redistribution pattern is captured, provided sufficiently large domains are chosen. The canonical rainfall distribution in response to global warming is similar to that shown in a CMIP3 study over tropical land by *Lintner et al.* [2012]. The rainfall sensitivities remain approximately constant for total rain, and for LR and MR, respectively in DCO2 and TCO2 (Table 1), indicating that the overall rainfall response may have reached quasi-steady state under both scenarios. However for heavy rain, the sensitivity is still evolving, with slightly reduced magnitude averaged for HR, but increased for averaged EHR from 27% K^{-1} to 32% K^{-1} between the two scenarios. We further note that the sensitivity of the most extreme rain events (rain rate > 60 mm/day) is more than double (from 46% to 102% K^{-1}) from DCO2 to TCO2 (compare Fig. S5 in the auxiliary material and Fig.2). These results suggest that the canonical rainfall response to CO_2 warming is highly nonlinear and scale selective, with increasing sensitivity in the most extremely heavy rain events as CO_2 emissions increase.

5. Geographic distributions

Geographic distributions are shown for the ensemble mean response for total rain, HR, MR and LR respectively (Fig. 3). Here, to emphasize model consistency, a grid-point ensemble value is displayed only if 10 or more models show the same sign of response. There is a large increase in total rain, most pronounced in climatologically wet regions of the tropics, especially over the equatorial western Pacific and the Asian monsoon regions including the northern Indian Ocean, South and Southeast Asia (Fig. 3a). Rainfall is also moderately increased over the extratropics of both hemispheres poleward of 50^{o} latitude. A general reduction of rainfall is found in the climatologically dry subtropical oceans, as well as in land regions of Central America and southwestern US, southern Europe/Mediterranean, and South Africa. The CMIP5 projected changes in total rain shown in Fig. 3a are consistent with the CMIP3 projected changes shown in the AR4 of IPCC (see Fig. 10.12a in IPCC 2007). Our analyses further indicate, as shown in Fig. 3b, most of the increased rainfall in the deep tropics is contributed by HR. Notably, very few regions experience a reduction in HR anywhere in the globe. This is akin to the outcome of throwing a loaded dice with heavy odds in favor of increased HR events due to global warming.

In contrast to HR, there is an overall reduction in MR over extensive regions in the subtropical and midlatitude oceans (Fig. 3c). Interestingly, significant increase of MR is found over high latitude land regions of North America and Eurasia, and the high latitude of the Southern Oceans (> 50^oS). It can also be seen that the anomalous dry regions over southwestern US, and southern Europe/Mediterranean noted previously (Fig. 3a) may be attributed to changes in MR. These features may reflect the change in storm tracks in conjunction with the poleward migration of the jestream induced by global warming [*Yin*, 2005; *Scheff and Frierson*, 2012]. Overall, LR (Fig. 3d) has a distribution similar but with opposite signs to those of MR. The presence of many regions where the collocated rainfall responses have different signs in HR, MR and/or LR may indicate change in the vertical structure of hydrometeors in clouds and rain systems over the regions [*Lau and Wu*, 2011].

For drought assessment, we use the first rain bin (< 0.024 mm day^{-1}) to represent trace amount or no-rain events. The occurrence of such an event at each grid location will be hereafter referred to as a “dry month” for that location. Using this definition, dry months occur about 3–10 % (ensemble mean = 5%) globally during the control period, but with negligible contribution to the rain amount (Fig. S1b in the auxiliary material). The geographical distribution of climatogically dry months simulated by the ensemble model mean (Fig. 4a) agrees reasonably well with that of the GPCP observation. Overall, the ensemble model mean over-estimates the aridity in subtropical land, but underestimates the dry oceanic stratocumulus zone off the west coast of Americas, and Africa (see Section S6 and Fig. S6 in the auxiliary material). From Fig.

4a, pronounced no-rain periods can be identified with deserts and arid regions of North Africa /Middle East/Pakistan, northwestern China, and southwestern US in NH, and South Africa, northwestern Australia, coastal central America, and northeastern Brazil in SH.

Under TCO2, the frequency of dry months in the ensemble mean increases by 16% at a rate of 4.7% K^{-1} globally. Our results regarding the increase in HR and drought are consistent with the study of *Giorgi et al.* [2011] who show a projected increase (4.8% K^{-1}) in the dry spell length as well as a general increase in hydroclimatic intensity from global model projections. Geographically, prolonged dry months occur predominantly over land areas in the subtropics or convective zones at the margins of climatological wet regions in both hemispheres (Fig. 4b). Specifically, the model ensemble projects a pronounced increase in dry months over a long and narrow east-west zone extending from North Africa/Mediterranean /Southern Europe to Iran, and over southern Africa. Prolonged dry months are also found in southwestern US/Mexico region, and northeastern Brazil. Much weaker dry zones are found over Southeast Asia and southern Australia. The dry regions generally coincide with reduced rainfall zones in the total rainfall distribution shown in Fig. 3a. However, because of the positive-definite nature of rainfall, a prolonged period of no rain in climatologically dry regions will not always show up as a major anomaly in a rainfall map (Fig. 3), but will be captured in a map of dry month distribution (Fig. 4). Hence, regions shown in Fig. 4b could be interpreted as those that have a higher risk of experiencing drought–like conditions under TCO2. Comparing with the model dry month climatology (Fig. 4a), the model ensemble projects under TCO2, an expansion of the desert or arid-zones, both equatorward and poleward, over major continental land regions. Again, CMIP5 models project no spatially coherent *reduction* in dry months anywhere in the globe, analogous to the outcome of throwing a loaded dice with overwhelming odds in favor of increased droughts due to global warming.

6. Conclusions

The IPCC CMIP5 models project a robust, canonical global response of rainfall characteristics to CO_2 warming, featuring an increase in heavy rain, a reduction in moderate rain, and an increase in light rain occurrence and amount globally. For a scenario of 1% CO_2 increase per year, the model ensemble mean projects at the time of approximately tripling of the CO_2 emissions, the probability of occurring of extremely heavy rain (monthly mean > 24 mm/day) will increase globally by 100–250%, moderate rain will decrease by 5–10% and light rain will increase by 10–15%. The increase in heavy rain is most pronounced in the equatorial central Pacific and the Asian monsoon regions. Moderate rain is reduced over extensive oceanic regions in the subtropics and extratropics, but increased over the extratropical land regions of North America, and Eurasia, and extratropical Southern Oceans. Light rain is mostly found to be inversely related to moderate rain locally, and with heavy rain in the central Pacific. The model ensemble also projects a significant global increase up to 16% more frequent in the occurrences of dry months (drought conditions), mostly over the subtropics as well as marginal convective zone in equatorial land regions, reflecting an expansion of the desert and arid-zones. The most pronounced increased risks of drought are found over an east-west fetch spanning North Africa, Mediterranean Sea, southern Europe to Iran, and another one over southern Africa. A secondary region of increased risk of drought is found over Southwest US/Mexico, and northeastern Brazil. Weak signals of increased drought signals are found over southern Australia, and Indo-China. The propensity for prolonged dry months over tropical land regions and marginal tropical convective zones over large landmass is most likely due to the fact that land regions are moisture limited from evaporation while oceanic regions are not. As a result, in a competition of moisture availability, the land regions lose out. This also suggests the importance of land-atmosphere feedback through changes in soil moisture and surface evaporation in leading to severe droughts [*Brubaker and Entekhabi*, 1996; *Sheffield and Wood*, 2008]. Also note that the increased risk of drought due to global warming can be exacerbated in regions undergoing large deforestation or land use change [*Lee et al.*, 2011].

Previous satellite data studies have identified correspondence of light, moderate and heavy rain types with warm rain/low clouds, mixed-phase rain/congestus, and ice-phase rain/high clouds respectively [*Lau and Wu*, 2007, 2011; *Masunaga and Kummerow*, 2006]. Hence, the canonical global rainfall response to CO_2 warming captured in the CMIP5 model projection suggests a global scale re-adjustment involving changes in circulation and rainfall characteristics, including possible teleconnection of extremely heavy rain and droughts separated by far distances (Lau and Kim, 2012). This adjustment is strongly constrained geographically by climatological rainfall pattern, and most likely by the GHG warming induced sea surface temperature anomalies (Xie et al., 2009) with unstable moister and warmer regions in the deep tropics getting more heavy rain, at the expense of nearby marginal convective zones in the tropics and stable dry zones in the subtropics. Our results are generally consistent with so-called "the rich-getting-richer, poor-getting-poorer" paradigm for precipitation response under global warming [*Allan et al.*, 2010; *Lau and Wu*, 2011; *Zhou et al.*, 2011; *Chou and Neelin*, 2004; *Chou et al.*, 2009]. We add that the increase in aridity in marginally convective zones in the tropical land under global warming is analogous to a "the-middle-class-also-getting-poorer" scenario. Further, our results suggest that there should be changes in rainfall types and cloud structures associated with a global shift in the climate norms induced by CO_2 warming. Ongoing studies (papers in preparation) by the authors have confirmed the importance of forcing from global warming induced anomalous sea surface temperature and vertical motions in governing the canonical spatial pattern of the global rainfall response to CO_2 warming. Finally, we stress that to better project future changes in rainfall characteristics and distribution, further work is needed to unravel the rainfall response to climate forcing not only from CO_2 and other greenhouse gases, but also from local and regional forcing such as sea surface temperature, aerosols, land use change, and dynamical feedback processes.

Acknowledgements: This work is partially funded by the Precipitation Measurement Missions (PMM) and the CMIP5 Diagnostic Project, Modeling and Analysis Program (MAP), NASA Headquarters. K.-M. Kim was also supported by the Korea Meteorological Administration Research and Development Program under grant CATER 2012-2062.

References

Allan, R. P., B. J. Soden, V. O. John, W. Ingram, and P. Good (2010), Current changes in tropical precipitation, *Environ. Res. Lett.*, doi:10.1088/1748-9326/5/52/025205.

Andrews, T., P. M. Forster, O. Boucher, N. Bellouin, and A. Jones (2010), Precipitation, radiative forcing and global temperature change, *Geophys. Res. Lett., 37*, L14701, doi:10.1029/2010GL043991.

Brubaker, K. L., and D. Entekhabi (1996), Analysis of feedback mechanisms in land-atmosphere interaction, *Water Resource Res*., *32*, 1343–1357.

Chou, C., and J. D. Neelin (2004), Mechanisms of global warming impacts on regional tropical precipitation, *J. Climatol.*, *17*, 2688–2701.

Chou, C., J. D. Neelin, C. A. Chen, and J. Y. Tu (2009), Evaluating the “rich-get-richer” mechanism in tropical precipitation change under global warming, *J. Clim.*, *22*, 1982–2005.

Chou, C., C.-A. Chen, P.-H. Tan, and K.-T. Chen (2012), Mechanisms for global warming impacts on precipitation frequency and intensity, *J. Clim.*, *25*, 3291–3306.

Field, C. B., et al. Eds. (2012), *Managing the Risks of Extreme Events and Disasters to Advance Climate Change Adaptation: Special Report of the Intergovernmental Panel on Climate Change*. http://ipcc-wg2.gov/SREX/

Frieler, K., M. Meinshausen, T. Schneider von Deimling, T. Andrews, and P. Forster (2011), Changes in global-mean precipitation in response to warming, greenhouse gas forcing and black carbon, *Geophys. Res. Lett., 38,* L04702, doi:10.1029/2010GL045953.

Giorgi, F., E. Coppola, E. S. Im, N. S. Diffenbaugh, X. Gao and Y. Shi (2011), Higher hydroclimatic intensity with global warming, *J. Clim.*, 24, 5309–5324.

Groisman, P. Ya., R. W. Knight, D. R. Easterling, T. R. Karl, G. C. Hergel, and V. N. Razuvaev (2005), Trends in intense precipitation in the climate record, *J. Clim.*, *18,* 1326–1350.

Held, I. M., and B. J. Soden (2006), Robust responses of the hydrological cycle to global warming, *J. Climate.*, *19*, 5686–5699.

Hu, Y., and Q. Fu (2007), Observed poleward expansion of the Hadley circulation since 1979, *Atmos. Chem. Phys.*, *7,* 5229–5236.

IPCC (2007), *Climate Change 2007: The Physical Science Basis. Contribution of Working Group I to the Fourth Assessment Report of the Intergovernmental Panel on Climate Change* [Solomon, S., D. Qin, M. Manning, Z. Chen, M. Marquis, K.B. Averyt, M. Tignor and H.L. Miller (eds.)]. *Cambridge University Press*, Cambridge, United Kingdom and New York, NY, USA, 996 pp.

Kharin, V., F. W. Zwiers, X. Zhang, and G. C. Hergerl (2007), Changes in temperature and precipitation extremes in IPCC ensemble of coupled model simulations, *J. Climate*, *20*, 1419–1444. DOI: 10.1175/JCLI4066.1

Lau, K.-M. and K.-M. Kim (2012), The 2010 Pakistan flood and Russian heat wave: Teleconnection of hydrometeorologic extremes, *J. Hydromet.*, *13*, 392–403.

Lau, K. M., and H.-T. Wu (2007), Detecting trends in tropical rainfall characteristics, 1979–2003, *Int. J. Climatol*., *27*, 979–988.

Lau, K.-M., and H.-T. Wu (2011), Climatology and changes in tropical oceanic rainfall characteristics inferred from Tropical Rainfall Measuring Mission (TRMM) data (1998–2009), *J. Geophys. Res.*, *116*, D17111, doi:10.1029/2011JD015827.

Lee, J.-E., B. R. Lintner, C. K. Boyce, and P. J. Lawrence (2011), Land use change exacerbates tropical South American drought by sea surface temperature variability, *Geophy. Res. Lett.*, *38*, L19706, doi:10.1029/2011GL049066.

Lintner, B. R., M. Biasutti, N. S. Diffenbaugh, J.-E. Lee, M. J. Niznik, and K. L. Findell (2012), Amplification of wet and dry month occurrence over tropical land regions in response to global warming, *J. Geophys. Res., 117*, D11106, doi:10.1029/2012JD017499.

Liu, C., R. P. Allan, and G. J. Huffman (2012), Co-variation of temperature and precipitation in CMIP5 models and satellite observations, *Geophys. Res. Lett., 39*, L13803, doi:10.1029/2012GL052093.

Masunaga, H., and C. D. Kummerow (2006), Observations of tropical precipitating clouds ranging from shallow to deep convective systems, *Geophy. Res. Lett.*, *33*, L16805, doi: 10.1029/2006GL026547.

Min, S.-K., X. Zhang, F. W. Zwiers, and G. C. Hegerl (2011), Human contribution to more intense precipitation extremes, *Nature*, *470*, 378–381.

O'Gorman, P. A., and T. Schneider (2009), The physical basis for increases in precipitation extremes in simulations of 21st-century climate change, *Proc. Natl. Acad. Sci. U. S. A.*, *106*, 14773–14777.

Riahi, K., S. Rao, V. Krey, C. Cho, V. Chirkov, G. Fischer, G. Kindermann, N. Nakicenovic, and P. Rafaj (2011), RCP 8.5—A scenario of comparatively high greenhouse gas emissions, *Climatic Change, 109*, 33–57.

Scheff, J., and D. M. Frierson (2012), Robust future precipitation declines in CMIP5 largely reflect the poleward expansion of model subtropical dry zones, *Geophys. Res. Lett., 39*, L18704, doi:10.1029/2012GL052910.

Seidel, D. J., Q. Fu, W. J. Randel, and T. J. Reichler (2008), Widening of the tropical belt in a changing climate, *Nat. Geosci*., *1*, 21–24.

Sheffield, J., and E. F. Wood (2008), Projected changes in drought occurrence under global warming from multi-model, multi-scenario IPCC AR4 simulations, *Clim. Dyn.*, *31*, 79–105.

Sun, F., M. L. Roderick, and G. D. Farquhar (2012), Changes in the variability of global land precipitation, *Geophys. Res. Lett., 39*, L19402, doi:10.1029/2012GL053369.

Taylor, K. E., R. J. Stouffer, and G. A. Meehl (2012), An overview of CMIP5 and the experiment design, *Bull. Amer. Meteor. Soc.*, *93*, 485–498.

Trenberth, K. E. (2011), Changes in precipitation with climate change, *Clim. Res., 47*, 123–138, doi:10.3354/cr00953.

Trenberth, K. E., A. Dai, R. M. Rasmussen, and D. B. Parsons (2003), The changing character of precipitation, *Bull. Amer. Meteor. Soc.*, *84*, 1205–1217.

Vecchi, G. A., B. J, Soden, A. T. Wittenberg, I. M. Held, A. Leetmaa, and M. J. Harrison (2006), Weakening of tropical Pacific atmospheric circulation due to anthropogenic forcing, *Nature*, *441*, 73–76.

Xie, S. P., C. Deser, G. Vecchi, J. Ma, H. Teng, and A. Wittterberg (2009), Global warming pattern formation: sea surface temperature and rainfall, *J. Clim., 23*, DOI:10.1175/2009JCLI3329.1.

Yin, J. H. (2005), A consistent poleward shift of the storm tracks in simulations of 21st century climate, *Geophys. Res. Lett., 32*, L18701, doi:10.1029/2005GL023684.

Zhou, Y. P., K.-M. Xu, Y. C. Sud, and A. K. Betts (2011), Recent trends of the tropical hydrological cycle inferred from Global Precipitation Climatology Project and International Satellite Cloud Climatology Project data, *J. Geophys. Res., 116*, D09101, doi:10.1029/2010JD015197.

Table 1. Sensitivity (dP/P/dT) of the ensemble-mean global (60°S to 60°N) precipitation to CO_2 induced warming for different rain types. Uncertainties are estimated from inter-model standard deviation for different rain types. Units are in % K^{-1}.

Rain types	*ALL*	*Extremely Heavy (EH)*	*Heavy (HR)*	*Moderate (MR)*	*Light (LR)*
DCO2	1.31± 0.38	26.8± 19.2	7.25± 2.32	-2.51± 0.62	1.86± 1.30
TCO2	1.35± 0.38	32.1± 26.6	6.98± 2.40	-2.51± 0.56	1.81± 1.27

Figure Captions

Figure 1. CMIP5 projections of changes in global mean surface temperature and precipitation induced by increased CO_2 emissions. Time series of global (60°S–60°N) annual mean (a) surface temperature and (b) rainfall from Year 1 to Year 140, based on experiment with 1% increase CO_2 emissions per year; (c) the difference in the zonal mean rain rate of the control and TCO2 for each of the 14 CMIP5 models as a function of latitude; and (d) the ensemble averaged zonal mean rain rates of the control (blue) and TCO2 (red), the ensemble-mean response (TCO2 minus control, black) and the inter-model 1-σ deviation (yellow shading).

Figure 2. Response in global (60°S–60°N) annual mean precipitation for TCO2 as a function of rain rate. (a) Change in the frequency of occurrence (FOC) and (b) sensitivity of precipitation amount to temperature change. Response of each of the 14 CMIP5 models is denoted by different color marks, and the model ensemble mean is denoted by the bar chart. Also shown in (a) are the ensemble mean FOC of the control and TCO2 (solid curves), in logarithmic scale.

Figure 3. Geographic distribution of the model ensemble-mean response in rain amount for TCO2. Changes in ensemble-mean annual accumulation (mm/year) for (a) total rain, (b) heavy rain, (c) moderate rain, and (d) light rain. Only regions with high consistency, *i.e*. responses of 10 or more out of the 14 CMIP5 models are of the same sign, are shown. All model outputs are interpolated to a common grid resolution (1.125^o longitude x 1.07^o latitude; 320 x 192 arrays).

Figure 4. Geographic distribution of the model ensemble annual dry-month duration (a) climatology, and (b) changes due to TCO2 scenario. Units are in number of dry months per year. Superimposed in (b) is the ensemble-mean precipitation (in mm/day) for the control period in contour lines. As in Fig. 3, only regions with high consistency are shown in (b).

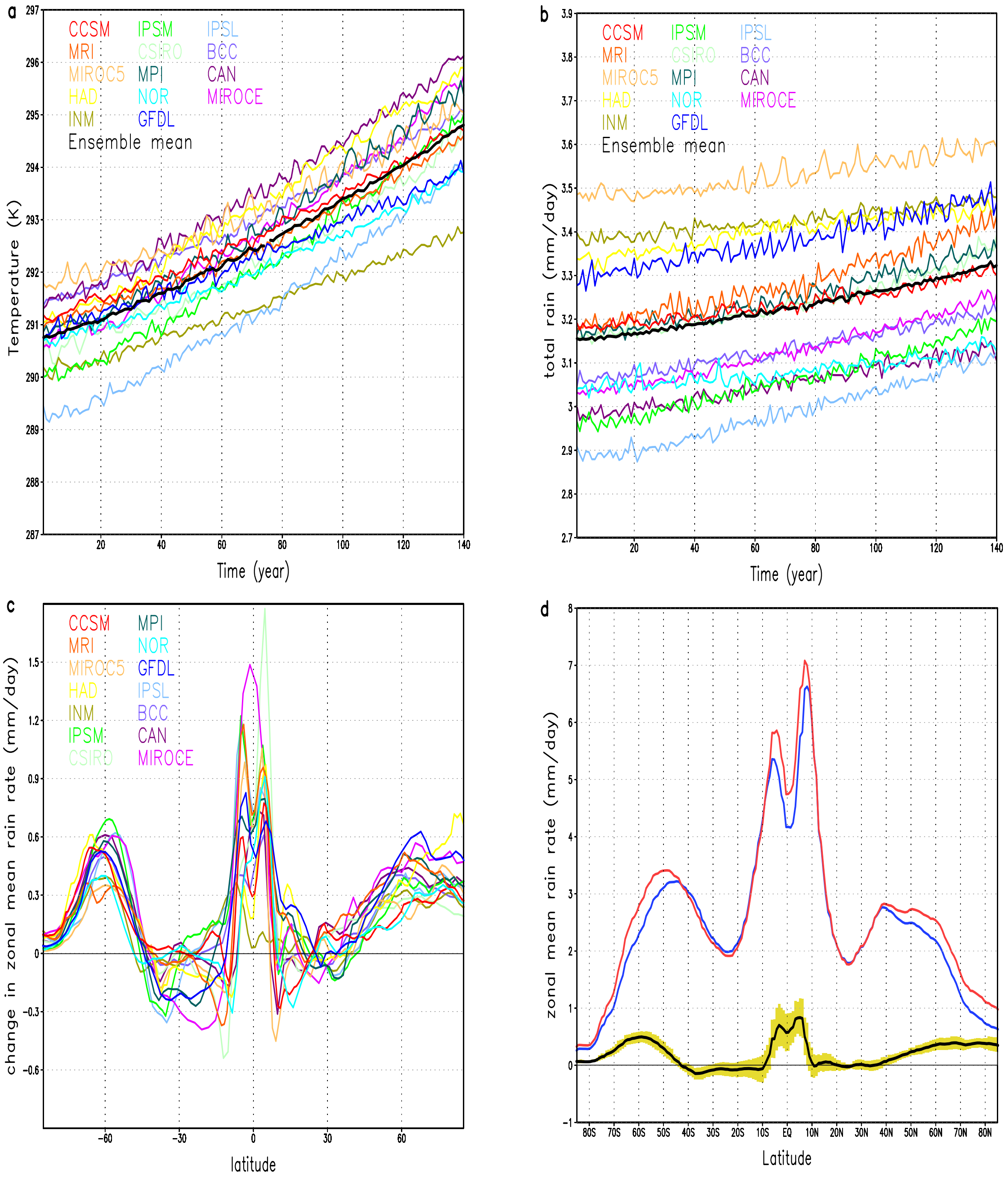
a
Temperature (K)
297
296
295
294
293
292
291
290
289
288
287
20
40
60
80
100
120
140
Time (year)
CCSM
IPSM
IPSL
MRI
CSIRO
BCC
MIROC5
MPI
CAN
HAD
NOR
MIROCE
INM
GFDL
Ensemble mean
b
total rain (mm/day)
3.9
3.8
3.7
3.6
3.5
3.4
3.3
3.2
3.1
3
2.9
2.8
2.7
20
40
60
80
100
120
140
Time (year)
CCSM
IPSM
IPSL
MRI
CSIRO
BCC
MIROC5
MPI
CAN
HAD
NOR
MIROCE
INM
GFDL
Ensemble mean
c
change in zonal mean rain rate (mm/day)
1.5
1.2
0.9
0.6
0.3
0
-0.3
-0.6
-60
-30
0
30
60
latitude
CCSM
MPI
MRI
NOR
MIROC5
GFDL
HAD
IPSL
INM
BCC
IPSM
CAN
CSIRO
MIROCE
d
zonal mean rain rate (mm/day)
8
7
6
5
4
3
2
1
0
-1
80S
70S
60S
50S
40S
30S
20S
10S
EQ
10N
20N
30N
40N
50N
60N
70N
80N
Latitude

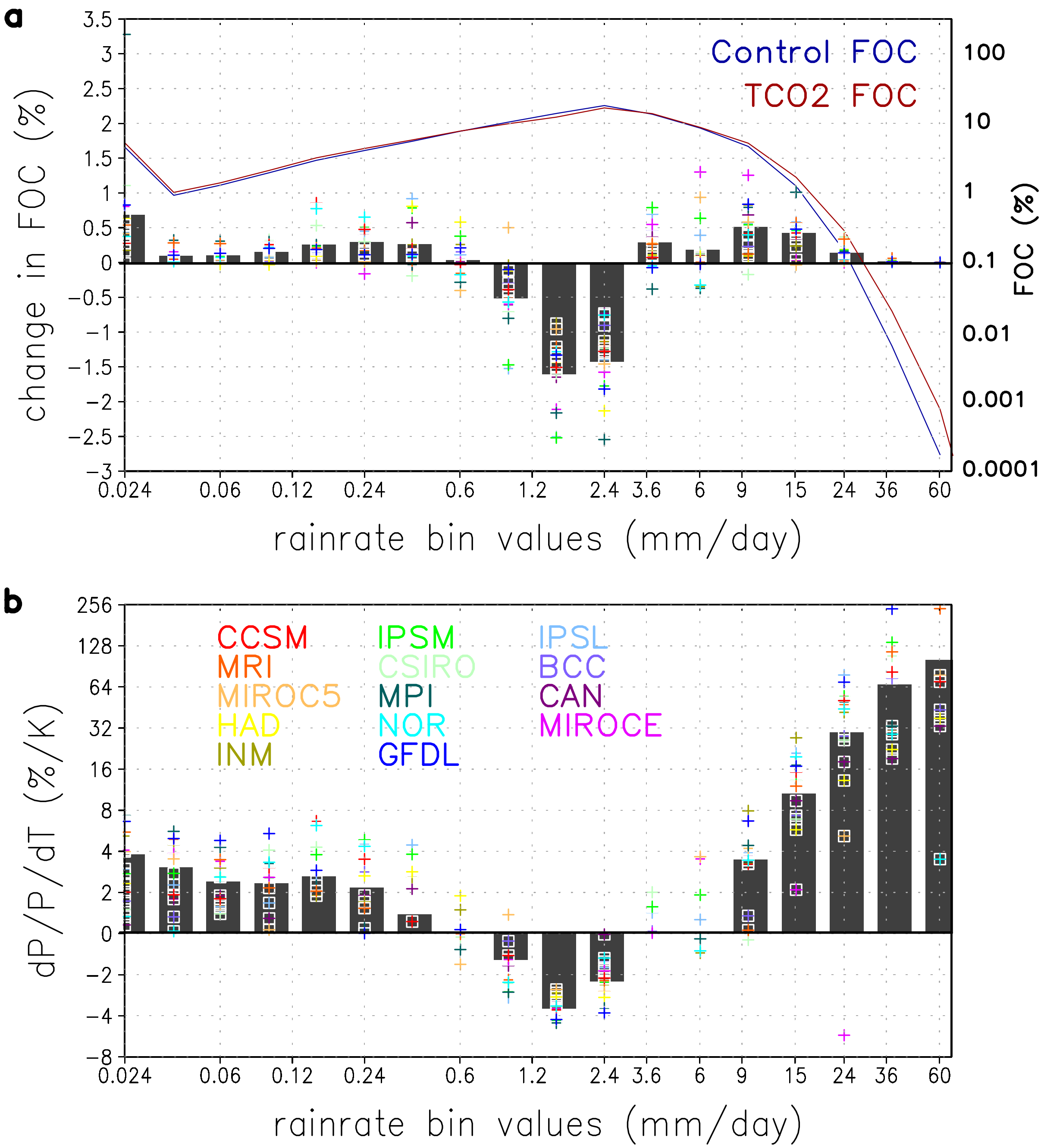
a
Control FOC
TCO2 FOC
change in FOC (%)
FOC (%)
3.5
3
2.5
2
1.5
1
0.5
0
−0.5
−1
−1.5
−2
−2.5
−3
100
10
1
0.1
0.01
0.001
0.0001
0.024
0.06
0.12
0.24
0.6
1.2
2.4
3.6
6
9
15
24
36
60
rainrate bin values (mm/day)
b
CCSM
MRI
MIROC5
HAD
INM
IPSM
CSIRO
MPI
NOR
GFDL
IPSL
BCC
CAN
MIROCE
dP/P/dT (%/K)
256
128
64
32
16
8
4
2
0
−2
−4
−8
0.024
0.06
0.12
0.24
0.6
1.2
2.4
3.6
6
9
15
24
36
60
rainrate bin values (mm/day)

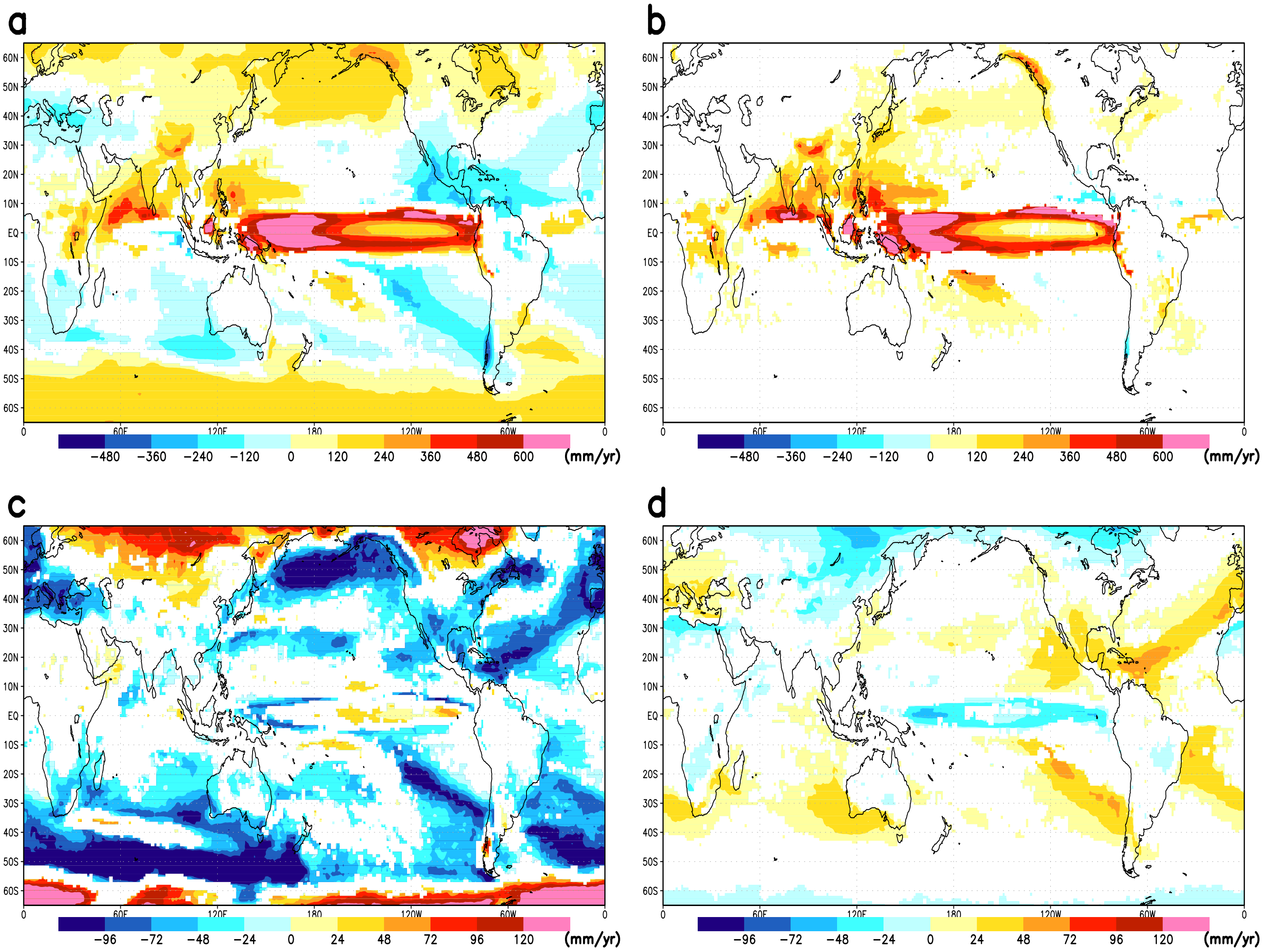
a
b
c
d
60N
50N
40N
30N
20N
10N
EQ
10S
20S
30S
40S
50S
60S
0
60E
120E
180
120W
60W
0
−480
−360
−240
−120
0
120
240
360
480
600
(mm/yr)
−96
−72
−48
−24
0
24
48
72
96
120
(mm/yr)

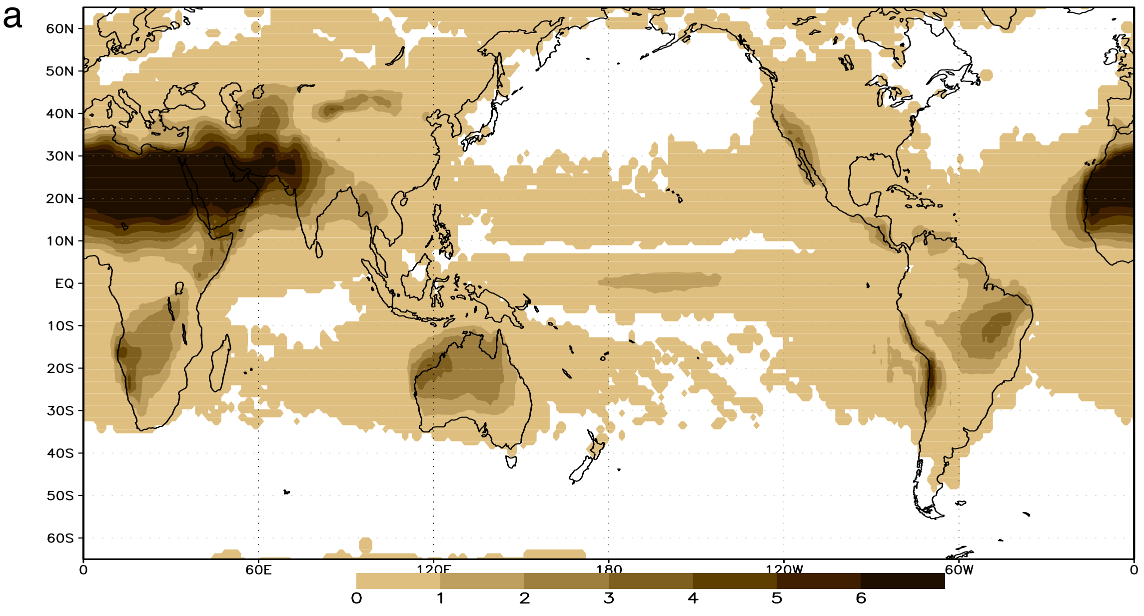
a
60N
50N
40N
30N
20N
10N
EQ
10S
20S
30S
40S
50S
60S
0
60E
120E
180
120W
60W
0
0
1
2
3
4
5
6

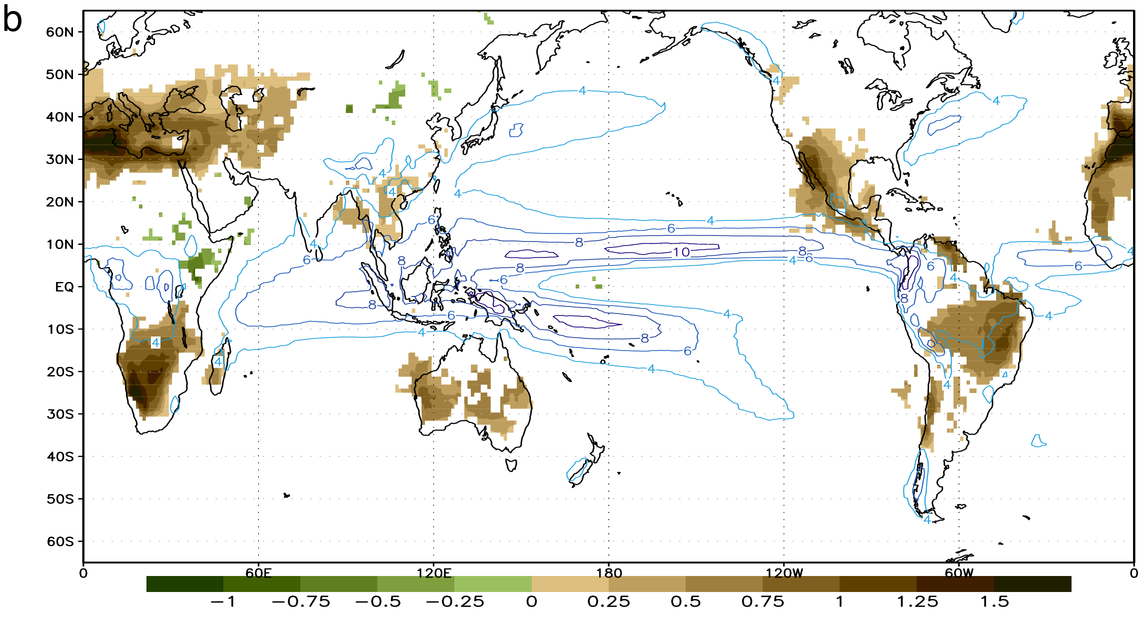
b
60N
50N
40N
30N
20N
10N
EQ
10S
20S
30S
40S
50S
60S
0
60E
120E
180
120W
60W
0
4
6
8
10
−1
−0.75
−0.5
−0.25
0
0.25
0.5
0.75
1
1.25
1.5